Current oscillations and intermittent emission near an electrode interface in a hybrid organic-inorganic perovskite single crystal

Hettiarachchi, Chathuranga; Xie, Aozhen; Nguyen, Tien Hoa; Yu, Junhong; Maddalena, Francesco; Dinh, Xuan Quyen; Muhammad Danang Birowosuto; Dang, Cuong

2019

Hettiarachchi, C., Xie, A., Nguyen, T. H., Yu, J., Maddalena, F., Dinh, X. Q., . . . Dang, C. (2019). Current oscillations and intermittent emission near an electrode interface in a hybrid organic-inorganic perovskite single crystal. ACS Applied Materials & Interfaces, 11(45), 42838-42845. doi:10.17645/mac.v7i4.2275

https://hdl.handle.net/10356/138197

https://doi.org/10.1021/acsami.9b15791

Current oscillations and intermittent emission near an electrode interface in hybrid organic-inorganic perovskite single crystal

Chathuranga Hettiarachchi, Aozhen Xie, Tien Hoa Nguyen, Junhong Yu, Francesco Maddalena, Xuan Quyen Dinh, Muhammad Danang Birowosuto, and Cuong Dang**

C. Hettiarachchi, A. Xie, J. Yu, C. Dang
School of Electrical and Electronic Engineering, The Photonics Institute (TPI), Nanyang Technological University, 50 Nanyang Avenue, Singapore 639798, Singapore
E-mail: hcdang@ntu.edu.sg

A. Xie, T. H. Nguyen, F. Maddalena, X. Q. Dinh, M. D. Birowosuto, C. Dang
CINTRA (CNRS−International−NTU-THALES-Research Alliances/UMI 3288), 50 Nanyang Drive, Singapore 637553, Singapore
Email: mbirowosuto@ntu.edu.sg

C. Hettiarachchi, A. Xie, C. Dang
Energy Research Institute @NTU (ERI@N), Nanyang Technological University, Research Techno Plaza, X-Frontier Block, Level 5, 50 Nanyang Drive, Singapore 637553, Singapore

X. Q. Dinh
R&T, Thales Solutions Asia Pte Ltd, 21 Changi North Rise, 498788, Singapore

Keywords: Perovskite single crystal LED, ionic conductance, metal-semiconductor-metal, current oscillation, intermittent emission, encapsulation.

Abstract

Hybrid organic–inorganic lead perovskites have great potential in optoelectronic device applications due to their high stability, narrow band emission, and strong luminescence. Single crystals with few defects are the best candidates to disclose a variety of interesting and important properties for light emitting device. Here we investigate a single crystalline $CH_3NH_3PbBr_3$ perovskite for its transport and electroluminescence properties. Simple fabrication method was used to obtain a 10±2 μm channel between two gold wire electrodes, which showed bright intermittent electroluminescence near the interface of one wire after cooling down with a constant biasing voltage. The active region of the perovskite single crystal was pristine, well isolated from surroundings through the fabrication to characterization process. Our presented sample provided an ideal condition to study bulk ionic-electronic properties of hybrid halide perovskites. At constant 6 V bias, the current through the sample shows

temperature dependent oscillation with Arrhenius behavior, suggesting a thermally activated process. The light emission from the sample experiences an intermittent emission rate of once every 26±6 minutes. Here we envisage that the current oscillations and intermittent emission are caused by ion mediated negative differential resistance and conductive filament formation respectively. The latter observation inspires future applications of the material from neuromorphic computing to the development of electroluminescence devices.

Introduction

Solution-processable hybrid halide perovskites have been proven as a promising semiconductor class for various optoelectronic applications. They have been shown with very high power conversion efficiencies in photovoltaic devices, reaching to date the certified efficiency[1] of over 23% and very high external quantum efficiencies of over 20% in light-emitting diodes (LEDs).[2,3] Researchers have also shown their high performance in other applications, such as X- and γ-ray scintillators[4–6], photo-detectors[7,8], non-volatile memories[9–11] field effect transistors[12–16] and even artificial synapses for neuromorphic computing. [17–19] Despite these remarkable characteristics, hybrid perovskites have also shown some drawbacks, such as surface restructuring on the aged surfaces,[20] poor operational stability and reproducibility[21,22] in devices. Perovskites are known to be ion conductors[23,24], and the ions can be mobilized by various factors[25] such as electric field[24], illumination[26], and chemical gradients.[27] However, other factors such as cation polarization, ferroelectric/ferroelastic distortion[28], traps or effects of air and moisture[20,29] can contribute to the instability of perovskite devices as well. Hence, a deeper understanding of material behaviors is needed to achieve high performance and stable devices. Current and electroluminescence from perovskite devices are observed to be subjected to intermittencies and hysteresis due to multiple imperfections in practical devices. Therefore, it is necessary to explore such devices at best encapsulated conditions to isolate its intrinsic behavior.

Recently, several studies have indicated that charge transport in polycrystalline hybrid lead halide perovskites is concurrently happening with ion migration, grain boundary effects, polarization disorder of the organic cations, and thermal vibrations of the inorganic lead halide octahedra.[12] In particular, it has become clear that ionic migration is the dominant factor at higher temperatures of above 160-180 K.[30,31] Nevertheless, the effect of charge transport in grain boundary in polycrystalline perovskites is still significant and interfere our interpretation. The study of single crystals[32,33] instead of polycrystalline thin films is necessary to simplify and isolate the effect of ionic migration. However, the crystals should be sufficiently thin to fabricate a device which is suitable for carrier injection in optoelectronic characterizations such as charge transport and electroluminescence.[34] Recently, light emission from single domain microcrystals with ITO/$CH_3NH_3PbBr_3$/Au structure[35] and thin encapsulated single crystals with ITO/$CH_3NH_3PbBr_3$/ITO structure[36] have been demonstrated up to room temperature. Recent result for light-emitting electrochemical cells of the Ag/$CH_3NH_3PbBr_3$/CNT structure also shows much faster intermittent emission rate of about 0.5 s.[37] However, they only observed one type of fluctuations and did not relate with a possible very slow intermittent emission in order of minutes or hours. In addition, there are still questions about the electroluminescence mechanism and the origins of second-long intermittent emission. Moreover, the effects related to surface-defects of the crystals, environmental effect (air, moisture) during the characterization or fabrication of the devices[38,39] are not negligible in these devices.

In this work, we demonstrate an approach to achieve a perovskite single crystal sample with entirely encapsulating the Au/$CH_3NH_3PbBr_3$/Au (metal/semiconductor/metal or MSM) architecture from the surrounding, where the electrodes and active perovskite single crystals stay pristine throughout the process from fabrication to characterization. Our approach with overgrown perovskite as a thick encapsulating layer is relatively simple and eliminates many factors affecting the sample. We use Gold(Au) as electrode material, which minimizes any oxidation during formation of the perovskite crystal.[40] This provides a better platform to study

the intrinsic bulk properties of the material. We observe a quasi-periodic on/off electroluminescence near the electrode interface with a cycle of 26±6 minutes at 160 K and 6 V constant bias, corresponding to fluctuation of electrical current between high (hundreds of μA) and low level (tens of μA), respectively. More interestingly, the electrical current oscillates in the time scale of seconds during the off period (low current) with temperature dependent frequency. Such regular and orderly quasi-periodic oscillation with period of seconds slows down when temperature decreases. We surmise that the quasi-periodic fluctuations in electroluminescence and current oscillation are behaviors of bulk single crystal perovskite, which is dominant in our proposed samples.

Experimental section

Preparation of gold electrodes: A silicon wafer (1 cm x 1 cm) with 2 μm thermal SiO_2 layer was used as a holder to grow the perovskite crystals with embedded electrodes. Two drops of acetic curable silicone sealant (Corning) were placed with 6±1 mm gap on top of the wafer to support the gold electrodes. Then, before the silicone is cured, two clean pieces of pure gold wire (diameter of 12.5±0.125 μm, 4±2 cm long) were held parallelly several microns apart in place. The gap between two wires were adjusted under the microscope. The sample was set aside for few hours for silicone to cure and firmly fix the position of two gold wires. The average length of the gap between the gold wires (electrodes) was confirmed by microscope as 10±2 μm.

Crystal Growth and sample fabrication: The sample was fabricated by enveloping the prefixed wire electrodes with a methylammonium lead bromide ($CH_3NH_3PbBr_3$) crystal. Methylammonium bromide and lead (II) bromide were mixed in 1:1 molar ratio, and dissolved in N, N-dimethylformamide with vigorous stirring to obtain a 1 mol/L solution. Once the solutes were completely dissolved, the precursor solution was filtered by a 0.2 μm pore size PTFE syringe filter and was subsequently transferred into several 25 mL vials. One vial was kept on a hotplate at 363 K to grow seed crystals. While the seed crystals are forming, a silicon wafer

with prefixed gold wires was transferred to the second vial containing the growth solution. When the seed crystals appear in first solution, one of the freshly grown seed crystal with about 1 mm^3 volume and cubic facets was transferred in to the second vial. The seed need to be placed close to the narrow channel between two gold wires using tweezers. The vial was then placed on a hotplate at 353 K to continue growing a large crystal from the seed. It is also important to avoid vibration or solution shaking as these would disturb the crystal growth. The process was allowed to continue until the $CH_3NH_3PbBr_3$ crystal completely enveloped the two gold wires.[41] Once the crystal is sufficiently large (more than 5 mm), the sample was removed from the growth solution and any residual solution is drained carefully with a tip of a wipe paper. The crystallographic data and the optical properties of the crystal after addition two wires are shown in Table S1 and Figure S1, respectively.

Current-voltage characterization: The gold wires, encapsulated by the perovskite crystal, were carefully soldered to a pair of sturdier wires, and silicone sealant was used to mechanically strengthen the connection. Subsequently, the sample was mounted in the cryo-chamber using silver paste at the back of the silicon wafer to ensure good thermal contact. Current-voltage (IV) curves were measured with Keithley 2400 source measurement unit.

Electroluminescence characterization: The sample was installed in a cryo-vacuum chamber, then pumped to a vacuum bellow 1mTorr. While a bias of 6 V was constantly applied, the sample was cooled down to 160 K. Such preconditioning process is introduced to obtain a frozen junction condition[35], where the mobile ions are allowed to reach a dynamic p-i-n structure and then reducing the back dissipation by cooling down the sample. The sample was operated only at the preconditioned polarity, to minimize the resetting of ion accumulation. The emission was coupled to a multimode fiber through two convex lenses and captured using an Ocean Optics USB HR4000 UV-Vis spectroscope. For electroluminescence (EL) imaging, Thorlabs CMOS DCC1645C camera with SZ11 microscope was used. For the light-current versus voltage (LIV) behavior, the light response was obtained by a photomultiplier tube (PMT)

biased at -1100 V. The EL signal from the PMT and the current signal captured through Femto DLPCA 200 current voltage trans-impedance amplifier was traced using a HP54615B oscilloscope.

Temperature dependent current-time characterization: In a separate experiment to record the temperature dependence of current oscillations, the current through the sample is captured in Femto DLPCA 200 and observed in oscilloscopes rolling mode screen. The sample temperature was changed while fixing a constant bias of 6 V, and the current has been captured at temperature interval of 10 K and saved to the computer. The frequency and deviation of the oscillation were calculated by averaging multiple periodic times for each temperature. For high frequency (i.e. in high temperatures) data, the number of spikes for a unit interval time was counted, averaged and reciprocated to obtain the frequency.

Results and discussion

The MSM structure of the Au/$CH_3NH_3PbBr_3$/Au where the gold wire electrodes were enveloped by a large perovskite single crystal is shown schematically in Figure 1a. The narrowest distance between two electrodes was very small (10±2 μm), while a large $CH_3NH_3PbBr_3$ perovskite crystal (5 mm) was grown around and completely covered the active electrode regions (more details in methods). Within a small region of 10±2 μm gap between electrodes, the perovskite semiconductor could be considered as a single crystalline structure. The well-encapsulated MSM sample with a high quality single crystalline perovskite allowed us to characterize the sample without much interference from crystal grain boundaries and surface states related to environmental effects, which are all well known to play crucial roles in perovskite samples. We expected a pure characterization of charge transfer and electroluminescence in bulk single crystalline perovskite materials.

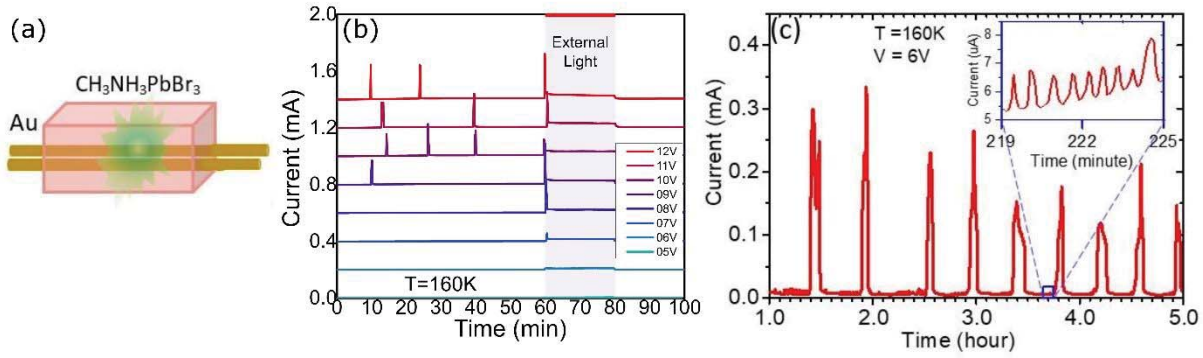

Figure 1. MSM sample structure with perovskite single crystal and its electrical behaviors. (a) Sketch of the sample, which is comprised of two gold wires embedded within a large hybrid halide perovskite single crystal. (b) Electrical current development behavior at different voltages, without any pre-conditioning while cooling down. For the clarity, each spectrum is shifted to the top of the other spectrum by 0.2 mA. (c) Electrical current behavior in long time at 6V constant bias, after preconditioning at same voltage while cooling down. Inset is a sample from the low current region (indicated in blue).

The electrical properties of the MSM structure were first investigated (Figure 1b) with an operation at a constant voltage and low temperatures, which has been cooled down to 160 K without applying any bias. The current gradually rose over 1-3 orders of magnitude, depending on the applied voltage, over the course of 30 minutes to 1 hour before stabilizing, as seen in Figure 1b. Brief current spikes (> 100 μA), lasting less than a minute, only occurred when the voltages were higher than 9 V. We also observed light emission from the single crystal, featuring a "blinking effect" correlated with sharp current spikes through the sample. No light emission was detected without the current spikes. Flashing external illumination white light on the sample, the photocurrent response was occurred as expected, however, with a brief current spike before stabilization. The electroluminescence can be observed associating with this brief current spike as well. After stopping the external illumination, the current decayed back to the normal level. Before the voltage was applied for each measurement, the sample had been kept without any bias for 5 minutes under a sun simulator lamp to minimize hysteresis effects between measurements.

However, when a bias voltage was applied before and during the cooling down process, the electrical behavior was very different. This implies that the material properties and electrical behaviors were susceptible to pre-conditioning of the sample. At the temperature of 160 K, current spikes (250±50 μA) were observed even at the bias of 6 V (pre-conditioning). The current spikes sustained in typically 4 minutes and returned to the lower current state (~tens of μA) with quasi-periodical repetition of 26±6 minutes of an interval as shown in Figure 1c. The different behaviors of a sample with and without pre-conditioning might relate to ion migration, which is well-known in perovskite semiconductor.[35] The applied bias voltage created electrical field and caused ions to migrate. However, the ion migration was faster at room temperature than that at cryogenic temperature. The ion migration would be settled down and this MSM sample behaved as a p-n junction device when reaching 160K temperature during pre-conditioning.[35] Without pre-conditioning, the ion migration happened at cryogenic temperatures would be very slow and require higher bias. As similar as the sample without pre-conditioning, electroluminescence (EL) signal was observed during the high current periods, while no EL was observed in the lower current state. The difference is only the smaller bias voltage for EL in the pre-conditioned sample.

Reducing the temperature was useful to reduce the mobile ions. However, the $MAPbBr_3$ undergoes a phase transition[42] around 150 K from tetragonal (I4/mcm) to orthorhombic ($Pna2_1$) via a transitional phase of tetragonal (P4/mmm). The phase transition of the perovskite crystal was reflected at its photoluminescence (PL) spectrum whose peak position was at the longest wavelength (547 nm) at 150-160 K (Figure S2). Hence, we limited the minimum temperature of the sample to 160 K to study the electroluminescence properties of the sample and material. Since the pre-conditioning was useful to establish the high current and EL without waiting time, we focused our experiments below for samples with pre-conditioning. We now look at the sample behaviors at two different regimes for the electric current through the sample at a

constant bias Voltage: high current spikes (~ hundreds of μA) and low current regions (~ tens of μA).

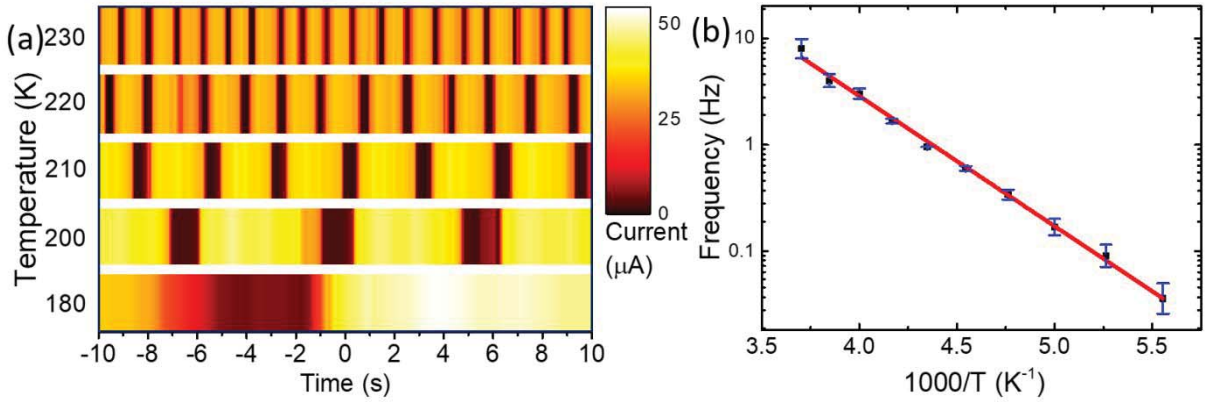

Figure 2. Current oscillation behaviors of the sample while cooling down. (a) The variation of current with time at different temperatures. (b) The dependence of current oscillation frequency on temperature: Arrhenius plot.

Considering the lower current regime, it is interesting that the electrical current through the sample showed an oscillation behavior with different periodicity depending on the temperature. Figure 2a and Figure S3 show these oscillatory behaviors investigated at different temperatures from 160 K to room temperature. The oscillation of the current was relatively slow at low temperatures, down to less than 0.100±0.050 Hz at T = 180 K or even 0.010±0.005 Hz observed at T = 160 K, see Figure 1c inset. However, the frequency of oscillation increased at higher temperatures. The trend continued up to room temperature, where the oscillations became relatively fast (above ~10 Hz). Together with higher contribution of random fluctuation at increasing temperatures, we can hardly notice the current oscillation at room temperature in oscilloscope trace. Plotting the logarithm of the oscillation frequency (f) versus the reciprocal of temperature T, as seen in Figure 2b, shows a typical Arrhenius behavior, $f(T) = A \cdot e^{-\frac{E_a}{RT}}$, where A is a constant pre-factor and R is the gas constant. Fitting the model, we deduced the activation energy E_a to be 23.4 kJ mol^{-1} (or 0.24 eV). The Arrhenius relationship between oscillation frequency and temperature suggests a thermally activated process. From this value, we extrapolate f(160 K) = 0.005±0.001 Hz, which is still consistent with the frequency obtained

from Figure 1c inset. To our knowledge, we are the first to report this oscillatory behavior in hybrid perovskite diodes. This is probably due to the encapsulation of the bulk perovskite channel within the perovskite single crystal, which eliminates surface and grain boundary effects that might be a source noise rendering this effect unobservable.

There are several possible mechanisms that might give rise to the thermally activated Arrhenius effect we observe. A likely possibility is ionic migration, which is which is widely reported in perovskites.[30,43–45] In such a case the activation energy is related to the hopping mechanism of the gold ions. Literature reports activation energies for MA^+ and Pb^{2+} of 0.58 eV and 2.31 eV, respectively[46]. The activation energy we obtain from our Arrhenius plot is of 0.24 eV, which is smaller compared to the other cations, suggesting that gold cations migrate much faster under the electric field and further corroborating the hypothesis that gold ions are main contributors to the filament formation.

Ionic motion also gives rise to a negative differential resistance (NDR) effects which are responsible for many oscillatory behaviors occurring at constant external stimuli, such as in electrochemical cells[47,48], Gunn diodes[49], neuron axon conductance[50] and plasma oscillations[51]. The origin of NDR characteristic could vary, ranging from an interface process to a spatiotemporal process. Usually, two types of carriers with different mobilities such as heavy vs. light electrons or electron vs. ion conductance could lead to spatiotemporal NDR. Interfacial NDR processes are related to a tunneling current, such as in tunneling diodes. Both charge carriers in perovskite[52] (electronic and ionic) could be the source of the oscillatory behavior, either it is a spatiotemporal process due to different mobilities; or modified electron-hole injection at metal semiconductor interfaces due to ion accumulation near the electrodes.

Another possibility to the origin of the oscillatory effect is electrochemical redox reactions at the gold electrode/perovskite interface, leading to the formation of the gold ions. These redox reactions would be thermally activated, frequency dependent, and are expected to feature the observed Arrhenius-like behavior. Examples of chemical reactions that show oscillatory

behavior, such as the redox Belousov–Zhabotinsky reaction [53,54], which often involve many complex reaction steps. The activation energy extracted from our measurements would then be determined by the activation energy of the slowest, limiting, reaction. Further investigation will however be necessary to fully understand he physical origin of the observed oscillatory behavior.

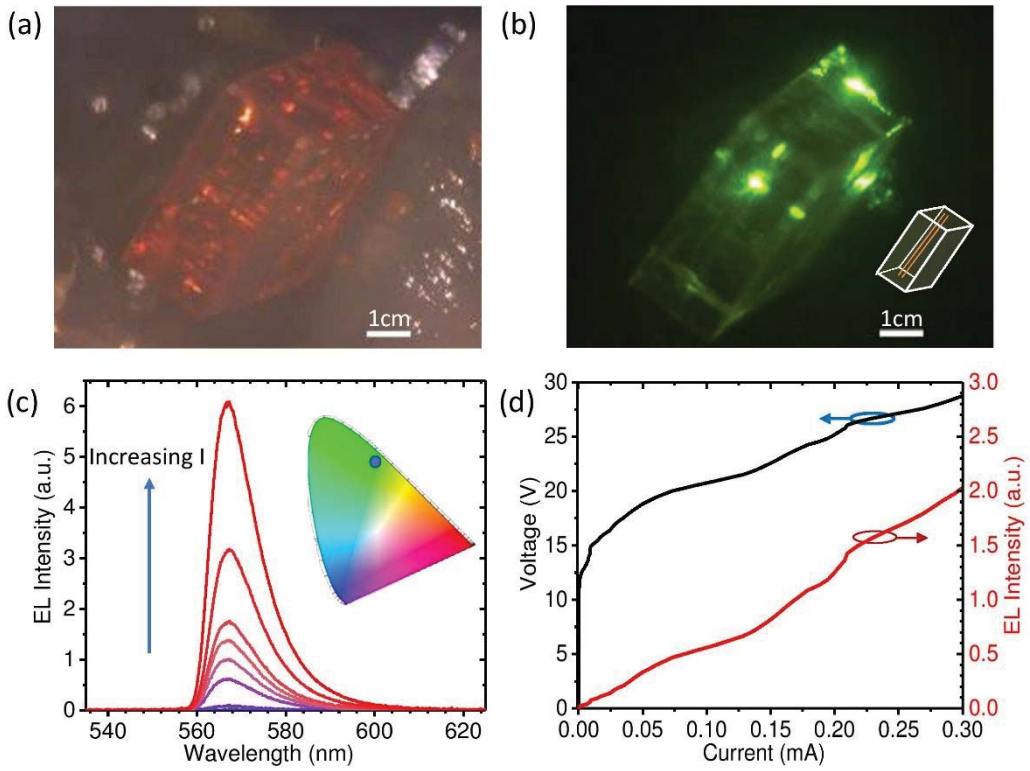

Figure 3. Electroluminescence characteristics. (a) Image of an actual sample under white light illumination. (b) The electroluminescence image of the sample and (inset) the crystal orientation. The bright emission spot in the middle of the image is within the crystal, at the narrow channel between two embedded gold wires. The other emission spots are due to internal reflections which scatter at the crystal surfaces and edges. Cuboid crystal orientation and placement of wires are sketched in the inset, as a guide to the eye. (c) Electroluminescence spectra at different currents. The inset shows the corresponding coordinate in CIE diagram. (d) LIV characteristics of the sample collected at 160K after leaving the sample for more than 5 minutes without a bias.

Looking at the higher current regime, we could observe bright green electroluminescence of $MAPbBr_3$ perovskite single crystal. Figure 3a and Figure 3b show the optical images of an actual MSM sample under white light illumination, and its electroluminescence associated with

current spikes, respectively. The Video S1 presents the electroluminescence of the same samples. The emission from the $CH_3NH_3PbBr_3$ originated in the narrow channel between two gold wires while the reflection in multiple surfaces of the perovskite crystal created virtually multiple bright spots around the crystal in the picture. The electroluminescence spectra of the single crystal perovskite MSM sample, shown in Figure 3c, featured a sharp (FWHM 12±1 nm) single peak at 563 nm with a steep rising edge around 560 nm. The chromaticity diagram in the inset of Figure 3c puts the emission in yellow-green range. The photoluminescence peak of $CH_3NH_3PbBr_3$ was at 537 nm at room temperature and shifted to 546 nm at 160 K (Figure S2). The difference between the EL and the PL spectra was attributed to self-absorption by the material. While PL was emitted from the surface of materials because the excitation laser could not penetrate deep inside the crystal, the EL was from the space between the two electrodes, which were deep inside the perovskite crystal. The captured EL spectrum was the result of EL passing through and being absorbed by a thick layer of material. Our experimental PL at room temperature with laser excitation from one side and PL collection from the other side of a crystal showed the similar spectral profile as that of EL (Figure S4). The significant red-shift of EL spectrum compared to PL spectrum was consistent with very strong self-absorption due to small Stokes shift in this bulk Perovskite material[55]. The asymmetry in the EL peaks, which can be fitted with an exponentially modified Gaussian profile (Figure S5), is another evidence for self-absorption at shorter wavelengths by the thick perovskite crystal.

With the pre-conditioned sample, the "current spikes" were occurring regularly with typically 4±1 minutes of 'on' time, which allowed us to characterize the electronic and optical properties of the sample. The Light-Current-Voltage (LIV) curves are presented in Figure 3d. The LIV behavior was similar to a typical light emitting diode with p-n junction and agreed well with other recent literature reports about single crystal perovskites under pre-conditioning[35,36]. The EL intensity correlated linearly with the current flowing though the sample, while IV curve showed a turn on voltage of about 6 V. The LIV results were measured with voltage sweeping

from 0 to 28 V at speed of 3.75 V/s in order to keep the consistency with the material condition. As presented in Figure 1c, the current was 250±50 μA at the current spikes when we applied a constant bias of 6 V. However, when we immediately swept the voltage the current only turned on and reached 200 μA at about 25 V. Hysteretic and history-dependent behavior is well known in hybrid perovskites, and attributed to ion segregation within the perovskite crystal[56].

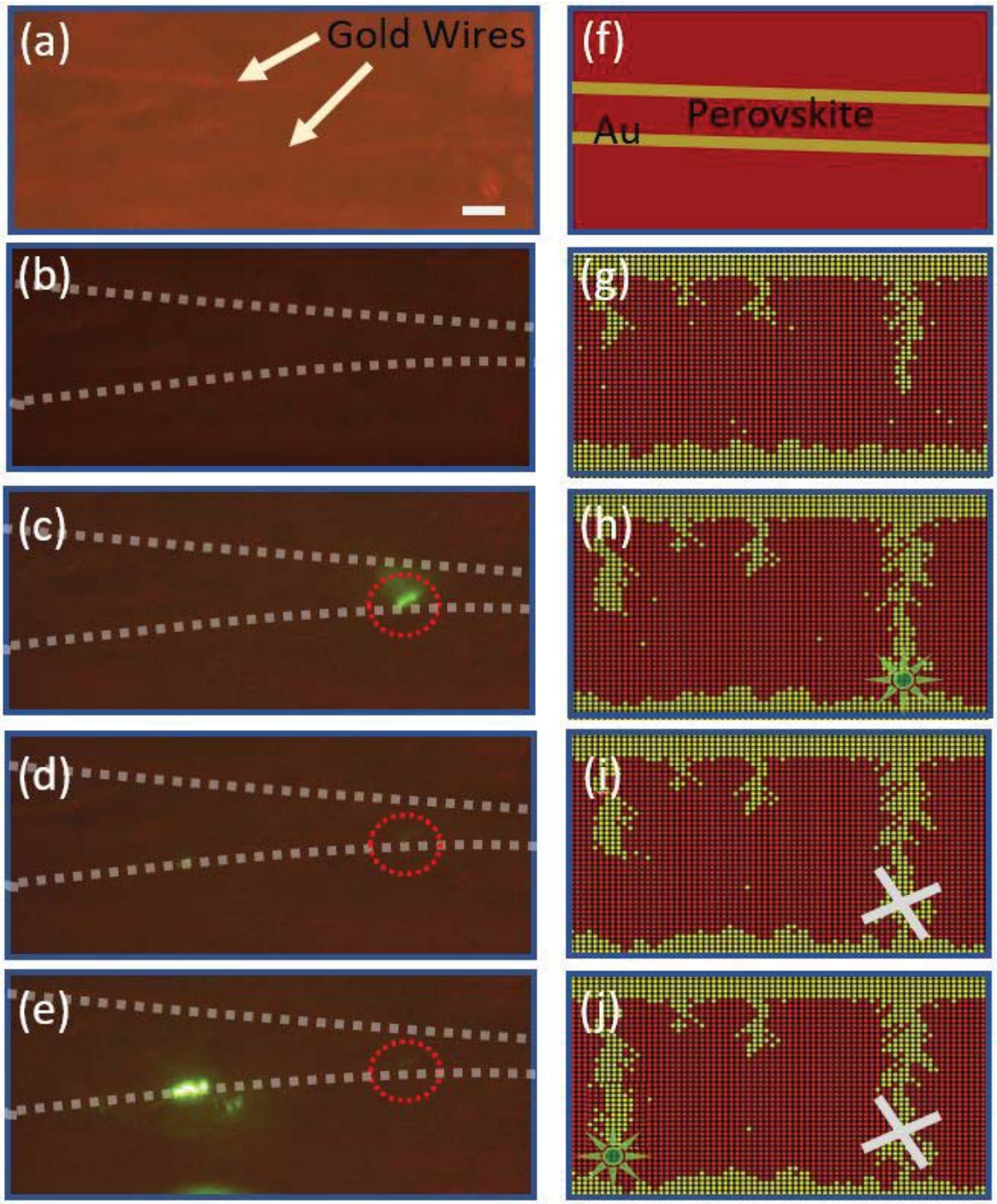

Figure 4. Local evolution of the emission within the perovskite crystal channel. (a) Close-up optical image of the channel under a bright external illumination. The gold wires with diameter 12.5 μm inside the crystal are slightly visible. Scale bar is 20 μm. (b-d) Emission localized at different positions within the channel. The appearance and dimming of emission at the red circled position due to growth of a filament and eventual burnout from short-circuit. (e) Emission is more prominent in a different place due to eventual formation of another filament. (f) Depiction of the encapsulated perovskite channel and (g-j) corresponding stages of illustrated filament formation/ destruction phenomenon within the channel. (not to scale). The star and the cross signs respectively indicate the filament positions where the emission appear, and eventually disappear due to filament short-circuit.

Besides the quasi-periodic current spikes concurrently happened with EL, our microscope images (Figure 4a – 4e and Video S2) showed that EL was only happened at the perovskite region near the anode side. To explain these observations, we empirically propose a simple model based on filament formation[57,58] driven by ionic motion, which is a known effect in lead halide perovskites.[59,60] The simulation procedure is discussed in Supporting Information Note S1, an illustration is presented in Figure 4f – 4j. In our model, gold (Au) atoms are oxidized at the anode, which is known for gold in perovskite, leading to gold ion migration.[61] The reduction of Au^+ into Au^0 is done by the electrons supplied by the cathode, similar to the electroplating effect. At the anode negative ions, i.e. Br^- will be oxidized into Br^0.Since oxidation of Au^0 into Au^+ at the anode occurs most likely by reduction of Pb^{2+} into Pb^0, the (molecular) bromine will most likely react with lead and form $PbBr_2$ rather than evaporate. [40,62] The formed Au^+ cations drift through the perovskite crystal to reach the cathode, hopping through interstitials or vacancy sites, following the electric field applied by external electrodes. Once the gold cations reach the cathode, gold cations will be further back to Au^0 atoms, which will be deposited on the cathode. The deposition of the gold atoms will modify the profile of the electric field, creating higher electric field at the tip of deposition position, hence leading more gold cations towards the tip and forming a filament of gold atoms as seen in Figure 4g. As the filament grows (Figure 4h), the local electric field increases and reaches a "threshold", the current sharply increases, similar to filament-based memory devices[58], causing the current surges in Figure 1b-c. The current density is high enough to have significant density of electrons and holes in the perovskite for radiative recombination, resulting in electroluminescence close to the other interface of the other gold electrode. The number of growth filaments, thickness and structure of the filaments could depend on various factors such as the voltage and temperature, ion diffusion constants and distance between the electrodes.[37,57] The electroluminescence will increase as the filament grows further, as seen in Figure 4c and Figure 4h. This type of filament formation has been

previously observed in perovskite devices, in particular in perovskite resistive memories.[63,64] However, the increases in current through a small perovskite gap when the filament approaches anode will also lead to a significant Joule heating, resulting into a sharp increase of the local temperature or even localized electrical breakdown as in Figure 4d and Figure 4i. This will lead to either the disintegration of the filament or damage to the local crystal structure of the perovskite. Thus, we can observe a sharp decrease in the current, and loss of electroluminescence. Eventually, another filament will form at a different position, repeating the process, as in Figure 4e and Figure 4j. However, this implies that the filament formation with the heating also can harm the material. Thus, at the same position, the material should not light-up again after the filament is broken. It is worth to note that the distance between our electrodes varies along the wire, and certainly the filament formation and EL happen around the smallest gap region where the electric field is the strongest. When the material at the narrowest position is damaged, another filament will grow at a nearest possible region.[37,57] This dual behavior of filament growth driven by the electric field, or "electrochemical metallization mechanism (ECM)" and filament breaking process due to heating, or "thermochemistry mechanism (TCM)" can be effective in respective processes due to low and high current regimes. In those regimes, the Joule heating at high currents can be highly concentrated at the filament, subjected to the limited heat dissipation through the bulk perovskite material.

Conclusion

We demonstrated a simple and robust single crystal perovskite sample, which showed electroluminescence at low temperatures and sufficiently high currents. The proposed sample concept where the electrode-perovskite structure stayed pristine throughout the process from fabrication to characterization allowed us to observe more regular current oscillation in single crystal perovskites. We observed a novel oscillatory behavior, which relates to thermally activated process because of its Arrhenius dependency on the temperature. In addition, the MSM sample showed a regular quasi-periodic sharp rise in current, corresponding to

intermittent electroluminescence, which can be explained by filament formation within the sample. These observations could shed new light on the intrinsic behaviors of single crystalline perovskite devices and highlight the significance of ionic motion on the conduction in perovskite devices, which is important to novel perovskite applications in future. While alerting the use of perovskite single crystals in normal lighting or communications applications, we hope the future will determine some practical uses of this interesting mechanism. Some possible areas are in iontronics, or in neuromorphic memory devices which can use the emission as an additional degree of freedom.

Supporting Information

Supporting Information is available free of charge on the ACS Publications website.

Temperature dependent photoluminescence (PL) spectra; current oscillation behavior at different temperatures; photoluminescence spectrum measured though the $CH_3NH_3PbBr_3$ crystal; electroluminescence spectrum and exponentially modified gaussian profile fitting; Monte-Carlo simulation procedure; single crystal X-ray diffraction (SCXRD) data; normalized absorbance spectrum.

Acknowledgements

We would like to thank the financial support from Singapore Ministry of Education Academic Research Fund Tier 1 MOE2017-T1-002-142 and Tier 1 MOE2016-T1-001-077. This project was also financially supported by the NRF (Singapore National Research Foundation) and the ANR (French research agency) through the international MULHYN (alias ACTIVE-NANOPHOT) funded project NRF2015-NRF-ANR000-MULHYN. We would thank Prof. Subodh Mhaisalkar, Executive Director of Energy Research Institute @ NTU (ERI@N) for supporting this work.

References

(1) NREL. Best Research-Cell Efficiencies https://www.nrel.gov/pv/assets/pdfs/pv-efficiency-chart.20181221.pdf (accessed Mar 1, 2019).

(2) Zhao, B.; Bai, S.; Kim, V.; Lamboll, R.; Shivanna, R.; Auras, F.; Richter, J. M.; Yang, L.; Dai, L.; Alsari, M.; She, X.-J.; Liang, L.; Zhang, J.; Lilliu, S.; Gao, P.; Snaith, H. J.; Wang, J.; Greenham, N. C.; Friend, R. H.; Di, D. High-Efficiency Perovskite–Polymer Bulk Heterostructure Light-Emitting Diodes. *Nat. Photonics* **2018**, *12* (12), 783–789. https://doi.org/10.1038/s41566-018-0283-4.

(3) Lin, K.; Xing, J.; Quan, L. N.; de Arquer, F. P. G.; Gong, X.; Lu, J.; Xie, L.; Zhao, W.; Zhang, D.; Yan, C.; Li, W.; Liu, X.; Lu, Y.; Kirman, J.; Sargent, E. H.; Xiong, Q.; Wei, Z. Perovskite Light-Emitting Diodes with External Quantum Efficiency Exceeding 20 per Cent. *Nature* **2018**, *562* (7726), 245–248. https://doi.org/10.1038/s41586-018-0575-3.

(4) Maddalena, F.; Tjahjana, L.; Xie, A.; Arramel; Zeng, S.; Wang, H.; Coquet, P.; Drozdowski, W.; Dujardin, C.; Dang, C.; Birowosuto, M. Inorganic, Organic, and Perovskite Halides with Nanotechnology for High–Light Yield X- and γ-Ray Scintillators. *Crystals* **2019**, *9* (2), 88. https://doi.org/10.3390/cryst9020088.

(5) Xie, A.; Nguyen, T. H.; Hettiarachchi, C.; Witkowski, M. E.; Drozdowski, W.; Birowosuto, M. D.; Wang, H.; Dang, C. Thermal Quenching and Dose Studies of X-Ray Luminescence in Single Crystals of Halide Perovskites. *J. Phys. Chem. C* **2018**, *122* (28), 16265–16273. https://doi.org/10.1021/acs.jpcc.8b03622.

(6) Birowosuto, M. D.; Cortecchia, D.; Drozdowski, W.; Brylew, K.; Lachmanski, W.; Bruno, A.; Soci, C. X-Ray Scintillation in Lead Halide Perovskite Crystals. *Sci. Rep.* **2016**, *6* (1), 37254. https://doi.org/10.1038/srep37254.

(7) Dou, L.; Yang, Y.; You, J.; Hong, Z.; Chang, W.-H.; Li, G.; Yang, Y. Solution-Processed Hybrid Perovskite Photodetectors with High Detectivity. *Nat. Commun.*

2014, *5* (1), 5404. https://doi.org/10.1038/ncomms6404.

(8) Yakunin, S.; Shynkarenko, Y.; Dirin, D. N.; Cherniukh, I.; Kovalenko, M. V. Non-Dissipative Internal Optical Filtering with Solution-Grown Perovskite Single Crystals for Full-Colour Imaging. *NPG Asia Mater.* **2017**, *9*, e431. https://doi.org/10.1038/am.2017.163.

(9) Gu, C.; Lee, J.-S. Flexible Hybrid Organic–Inorganic Perovskite Memory. *ACS Nano* **2016**, *10* (5), 5413–5418. https://doi.org/10.1021/acsnano.6b01643.

(10) Ma, H.; Wang, W.; Xu, H.; Wang, Z.; Tao, Y.; Chen, P.; Liu, W.; Zhang, X.; Ma, J.; Liu, Y. Interface State-Induced Negative Differential Resistance Observed in Hybrid Perovskite Resistive Switching Memory. *ACS Appl. Mater. Interfaces* **2018**, *10* (25), 21755–21763. https://doi.org/10.1021/acsami.8b07850.

(11) Guan, X.; Hu, W.; Haque, M. A.; Wei, N.; Liu, Z.; Chen, A.; Wu, T. Light-Responsive Ion-Redistribution-Induced Resistive Switching in Hybrid Perovskite Schottky Junctions. *Adv. Funct. Mater.* **2018**, *28* (3), 1704665. https://doi.org/10.1002/adfm.201704665.

(12) Senanayak, S. P.; Yang, B.; Thomas, T. H.; Giesbrecht, N.; Huang, W.; Gann, E.; Nair, B.; Goedel, K.; Guha, S.; Moya, X.; McNeill, C. R.; Docampo, P.; Sadhanala, A.; Friend, R. H.; Sirringhaus, H. Understanding Charge Transport in Lead Iodide Perovskite Thin-Film Field-Effect Transistors. *Sci. Adv.* **2017**, *3* (1), e1601935. https://doi.org/10.1126/sciadv.1601935.

(13) Maddalena, F.; Chin, X. Y.; Cortecchia, D.; Bruno, A.; Soci, C. Brightness Enhancement in Pulsed-Operated Perovskite Light-Emitting Transistors. *ACS Appl. Mater. Interfaces* **2018**, *10* (43), 37316–37325. https://doi.org/10.1021/acsami.8b11057.

(14) Chin, X. Y.; Cortecchia, D.; Yin, J.; Bruno, A.; Soci, C. Lead Iodide Perovskite Light-Emitting Field-Effect Transistor. *Nat. Commun.* **2015**, *6*, 7383.

https://doi.org/10.1038/ncomms8383.

(15) Maddalena, F.; Boix, P. P.; Xin Yu, C.; Mathews, N.; Soci, C.; Mhaisalkar, S. Charge Transport in Organometal Halide Perovskites. In *Organic-Inorganic Halide Perovskite Photovoltaics*; Park, N.-G., Grätzel, M., Miyasaka, T., Eds.; Springer International Publishing: Cham, 2016; pp 201–222. https://doi.org/10.1007/978-3-319-35114-8_8.

(16) Yu, W.; Li, F.; Yu, L.; Niazi, M. R.; Zou, Y.; Corzo, D.; Basu, A.; Ma, C.; Dey, S.; Tietze, M. L.; Buttner, U.; Wang, X.; Wang, Z.; Hedhili, M. N.; Guo, C.; Wu, T.; Amassian, A. Single Crystal Hybrid Perovskite Field-Effect Transistors. *Nat. Commun.* **2018**, 1–10. https://doi.org/10.1038/s41467-018-07706-09.

(17) Xiao, Z.; Huang, J. Energy-Efficient Hybrid Perovskite Memristors and Synaptic Devices. *Adv. Electron. Mater.* **2016**, *2* (7), 1–8. https://doi.org/10.1002/aelm.201600100.

(18) Choi, J.; Han, J. S.; Hong, K.; Kim, S. Y.; Jang, H. W. Organic-Inorganic Hybrid Halide Perovskites for Memories, Transistors, and Artificial Synapses. *Adv. Mater.* **2018**, *30* (42), 1704002. https://doi.org/10.1002/adma.201704002.

(19) John, R. A.; Yantara, N.; Ng, Y. F.; Narasimman, G.; Mosconi, E.; Meggiolaro, D.; Kulkarni, M. R.; Gopalakrishnan, P. K.; Nguyen, C. A.; De Angelis, F.; Mhaisalkar, S. G.; Basu, A.; Mathews, N. Ionotronic Halide Perovskite Drift-Diffusive Synapses for Low-Power Neuromorphic Computation. *Adv. Mater.* **2018**, *30* (51), 1805454. https://doi.org/10.1002/adma.201805454.

(20) Murali, B.; Dey, S.; Abdelhady, A. L.; Peng, W.; Alarousu, E.; Kirmani, A. R.; Cho, N.; Sarmah, S. P.; Parida, M. R.; Saidaminov, M. I.; Zhumekenov, A. A.; Sun, J.; Alias, M. S.; Yengel, E.; Ooi, B. S.; Amassian, A.; Bakr, O. M.; Mohammed, O. F. Surface Restructuring of Hybrid Perovskite Crystals. *ACS Energy Lett.* **2016**, acsenergylett.6b00517. https://doi.org/10.1021/acsenergylett.6b00517.

(21) Schelhas, L. T.; Li, Z.; Christians, J. A.; Goyal, A.; Kairys, P.; Harvey, S. P.; Kim, D.

H.; Stone, K. H.; Luther, J. M.; Zhu, K.; Stevanovic, V.; Berry, J. J. Insights into Operational Stability and Processing of Halide Perovskite Active Layers. *Energy Environ. Sci.* **2019**, *12* (4), 1341–1348. https://doi.org/10.1039/C8EE03051K.

(22) Christians, J. A.; Habisreutinger, S. N.; Berry, J. J.; Luther, J. M. Stability in Perovskite Photovoltaics: A Paradigm for Newfangled Technologies. *ACS Energy Lett.* **2018**, *3* (9), 2136–2143. https://doi.org/10.1021/acsenergylett.8b00914.

(23) Vicente, N.; Garcia-Belmonte, G. Organohalide Perovskites Are Fast Ionic Conductors. *Adv. Energy Mater.* **2017**, *7* (19), 1700710. https://doi.org/10.1002/aenm.201700710.

(24) Mizusaki, J.; Arai, K.; Fueki, K. Ionic Conduction of the Perovskite-Type Halides. *Solid State Ion.* **1983**, *11* (3), 203–211. https://doi.org/10.1016/0167-2738(83)90025-5.

(25) Walsh, A.; Stranks, S. D. Taking Control of Ion Transport in Halide Perovskite Solar Cells. *ACS Energy Lett.* **2018**, *3* (8), 1983–1990. https://doi.org/10.1021/acsenergylett.8b00764.

(26) Galisteo-López, J. F.; Li, Y.; Míguez, H. Three-Dimensional Optical Tomography and Correlated Elemental Analysis of Hybrid Perovskite Microstructures: An Insight into Defect-Related Lattice Distortion and Photoinduced Ion Migration. *J. Phys. Chem. Lett.* **2016**, *7* (24), 5227–5234. https://doi.org/10.1021/acs.jpclett.6b02456.

(27) Shewmon, N. T.; Yu, H.; Constantinou, I.; Klump, E.; So, F. Formation of Perovskite Heterostructures by Ion Exchange. *ACS Appl. Mater. Interfaces* **2016**, *8* (48), 33273–33279. https://doi.org/10.1021/acsami.6b10034.

(28) Liu, Y.; Collins, L.; Proksch, R.; Kim, S.; Watson, B. R.; Doughty, B.; Calhoun, T. R.; Ahmadi, M.; Ievlev, A. V.; Jesse, S.; Retterer, S. T.; Belianinov, A.; Xiao, K.; Huang, J.; Sumpter, B. G.; Kalinin, S. V.; Hu, B.; Ovchinnikova, O. S. Chemical Nature of Ferroelastic Twin Domains in $CH_3NH_3PbI_3$ Perovskite. *Nat. Mater.* **2018**, *17* (11), 1013–1019. https://doi.org/10.1038/s41563-018-0152-z.

(29) Kollár, M.; Ćirić, L.; Dil, J. H.; Weber, A.; Muff, S.; Ronnow, H. M.; Náfrádi, B.;

Monnier, B. P.; Luterbacher, J. S.; Forró, L.; Horváth, E. Clean, Cleaved Surfaces of the Photovoltaic Perovskite. *Sci. Rep.* **2017**, *7* (1), 695. https://doi.org/10.1038/s41598-017-00799-0.

(30) Li, C.; Guerrero, A.; Zhong, Y.; Gräser, A.; Luna, C. A. M.; Köhler, J.; Bisquert, J.; Hildner, R.; Huettner, S. Real-Time Observation of Iodide Ion Migration in Methylammonium Lead Halide Perovskites. *Small* **2017**, *13* (42), 1701711. https://doi.org/10.1002/smll.201701711.

(31) Birkhold, S. T.; Precht, J. T.; Liu, H.; Giridharagopal, R.; Eperon, G. E.; Schmidt-Mende, L.; Li, X.; Ginger, D. S. Interplay of Mobile Ions and Injected Carriers Creates Recombination Centers in Metal Halide Perovskites under Bias. *ACS Energy Lett.* **2018**, *3* (6), 1279–1286. https://doi.org/10.1021/acsenergylett.8b00505.

(32) Saidaminov, M. I.; Abdelhady, A. L.; Murali, B.; Alarousu, E.; Burlakov, V. M.; Peng, W.; Dursun, I.; Wang, L.; He, Y.; Maculan, G.; Goriely, A.; Wu, T.; Mohammed, O. F.; Bakr, O. M. High-Quality Bulk Hybrid Perovskite Single Crystals within Minutes by Inverse Temperature Crystallization. *Nat. Commun.* **2015**, *6*, 7586. https://doi.org/10.1038/ncomms8586.

(33) Zhang, T.; Yang, M.; Benson, E. E.; Li, Z.; van de Lagemaat, J.; Luther, J. M.; Yan, Y.; Zhu, K.; Zhao, Y. A Facile Solvothermal Growth of Single Crystal Mixed Halide Perovskite $CH_3NH_3Pb(Br_{1-x}Cl_x)_3$. *Chem. Commun.* **2015**, *51* (37), 7820–7823. https://doi.org/10.1039/C5CC01835H.

(34) Lv, Q.; Lian, Z.; He, W.; Sun, J. L.; Li, Q.; Yan, Q. A Universal Top-down Approach toward Thickness-Controllable Perovskite Single-Crystalline Thin Films. *J. Mater. Chem. C* **2018**, *6* (16), 4464–4470. https://doi.org/10.1039/c8tc00842f.

(35) Chen, M.; Shan, X.; Geske, T.; Li, J.; Yu, Z. Manipulating Ion Migration for Highly Stable Light-Emitting Diodes with Single-Crystalline Organometal Halide Perovskite Microplatelets. *ACS Nano* **2017**, *11* (6), 6312–6318.

https://doi.org/10.1021/acsnano.7b02629.

(36) Nguyen, V.; Katsuki, H.; Sasaki, F.; Yanagi, H. Single-Crystal Perovskite $CH_3NH_3PbBr_3$ Prepared by Cast Capping Method for Light-Emitting Diodes. *Jpn. J. Appl. Phys.* **2018**, *57* (4S), 04FL10. https://doi.org/10.7567/JJAP.57.04FL10.

(37) Andričević, P.; Mettan, X.; Kollár, M.; Náfrádi, B.; Sienkiewicz, A.; Garma, T.; Rossi, L.; Forró, L.; Horváth, E. Light-Emitting Electrochemical Cells of Single Crystal Hybrid Halide Perovskite with Vertically Aligned Carbon Nanotubes Contacts. *ACS Photonics* **2019**, *6* (4), 967–975. https://doi.org/10.1021/acsphotonics.8b01653.

(38) Murali, B.; Yengel, E.; Yang, C.; Peng, W.; Alarousu, E.; Bakr, O. M.; Mohammed, O. F. The Surface of Hybrid Perovskite Crystals: A Boon or Bane. *ACS Energy Lett.* **2017**, *2* (4), 846–856. https://doi.org/10.1021/acsenergylett.6b00680.

(39) Grancini, G.; D'Innocenzo, V.; Dohner, E. R.; Martino, N.; Srimath Kandada, A. R.; Mosconi, E.; De Angelis, F.; Karunadasa, H. I.; Hoke, E. T.; Petrozza, A. $CH_3NH_3PbI_3$ Perovskite Single Crystals: Surface Photophysics and Their Interaction with the Environment. *Chem. Sci.* **2015**, *6* (12), 7305–7310. https://doi.org/10.1039/C5SC02542G.

(40) Zhao, L.; Kerner, R. A.; Xiao, Z.; Lin, Y. L.; Lee, K. M.; Schwartz, J.; Rand, B. P. Redox Chemistry Dominates the Degradation and Decomposition of Metal Halide Perovskite Optoelectronic Devices. *ACS Energy Lett.* **2016**, *1* (3), 595–602. https://doi.org/10.1021/acsenergylett.6b00320.

(41) Hettiarachchi, C.; Birowosuto, M. D.; Nguyen, T. H.; Ahmad, R.; Pita, K.; Mathews, N.; Dang, C. Solution Grown Double Heterostructure on a Large Hybrid Halide Perovskite Crystal. *CrystEngComm* **2018**, *20* (42), 6653–6661. https://doi.org/10.1039/C8CE01298A.

(42) Chen, C.; Hu, X.; Lu, W.; Chang, S.; Shi, L.; Li, L.; Zhong, H.; Han, J.-B. Elucidating the Phase Transitions and Temperature-Dependent Photoluminescence of $MAPbBr_3$

Single Crystal. *J. Phys. D. Appl. Phys.* **2018**, *51* (4), 045105. https://doi.org/10.1088/1361-6463/aaa0ed.

(43) Halder, A.; Pathoor, N.; Chowdhury, A.; Sarkar, S. K. Photoluminescence Flickering of Micron-Sized Crystals of Methylammonium Lead Bromide: Effect of Ambience and Light Exposure. *J. Phys. Chem. C* **2018**, *122* (27), 15133–15139. https://doi.org/10.1021/acs.jpcc.8b03862.

(44) Li, C.; Guerrero, A.; Huettner, S.; Bisquert, J. Unravelling the Role of Vacancies in Lead Halide Perovskite through Electrical Switching of Photoluminescence. *Nat. Commun.* **2018**, *9* (1), 5113. https://doi.org/10.1038/s41467-018-07571-6.

(45) Zhang, H.; Lin, H.; Liang, C.; Liu, H.; Liang, J.; Zhao, Y.; Zhang, W.; Sun, M.; Xiao, W.; Li, H.; Polizzi, S.; Li, D.; Zhang, F.; He, Z.; Choy, W. C. H. Organic-Inorganic Perovskite Light-Emitting Electrochemical Cells with a Large Capacitance. *Adv. Funct. Mater.* **2015**, *25* (46), 7226–7232. https://doi.org/10.1002/adfm.201502962.

(46) Lee, J.-W.; Kim, S.-G.; Yang, J.-M.; Yang, Y.; Park, N.-G. Verification and Mitigation of Ion Migration in Perovskite Solar Cells. *APL Mater.* **2019**, *7* (4), 041111. https://doi.org/10.1063/1.5085643.

(47) López-Sauri, D. A.; Veleva, L.; Pérez-Ángel, G. Potentiostatic Current and Galvanostatic Potential Oscillations during Electrodeposition of Cadmium. *Phys. Chem. Chem. Phys.* **2015**, *17* (34), 22266–22271. https://doi.org/10.1039/C5CP03253A.

(48) Bai, H.; Qing, S.; Yang, D.; Zhang, Y.; Fan, X.; Tao, C. Periodic Potential Oscillation during Oxygen Evolution Catalyzed by Manganese Oxide at Constant Current. *J. Electrochem. Soc.* **2017**, *164* (4), E78–E83. https://doi.org/10.1149/2.1241704jes.

(49) Yngvesson, S. Transferred Electron Devices (TED) — Gunn Devices. In *Microwave Semiconductor Devices*; Springer US: Boston, MA, 1991; pp 23–58. https://doi.org/10.1007/978-1-4615-3970-4_2.

(50) Gerstner, W.; Kistler, W. M. *Spiking Neuron Models*; Cambridge University Press: Cambridge, 2002. https://doi.org/10.1017/CBO9780511815706.

(51) Kumar, R.; Narayanan, R.; Prasad, A. Hysteresis in Amplitudes of Self-Excited Oscillations for Co-Axial Electrode-Geometry DC Glow Discharge Plasma. *Phys. Plasmas* **2014**, *21* (12). https://doi.org/10.1063/1.4901578.

(52) Yang, T.-Y.; Gregori, G.; Pellet, N.; Grätzel, M.; Maier, J. The Significance of Ion Conduction in a Hybrid Organic-Inorganic Lead-Iodide-Based Perovskite Photosensitizer. *Angew. Chemie Int. Ed.* **2015**, *54* (27), 7905–7910. https://doi.org/10.1002/anie.201500014.

(53) Gyorgyi, L.; Turanyi, T.; Field, R. J. Mechanistic Details of the Oscillatory Belousov-Zhabotinskii Reaction. *J. Phys. Chem.* **1990**, *94* (18), 7162–7170. https://doi.org/10.1021/j100381a039.

(54) Aller Pellitero, M.; Álvarez Lamsfus, C.; Borge, J. The Belousov–Zhabotinskii Reaction: Improving the Oregonator Model with the Arrhenius Equation. *J. Chem. Educ.* **2013**, *90* (1), 82–89. https://doi.org/10.1021/ed300227w.

(55) Karki, K. J.; Abdellah, M.; Zhang, W.; Pullerits, T. Different Emissive States in the Bulk and at the Surface of Methylammonium Lead Bromide Perovskite Revealed by Two-Photon Micro-Spectroscopy and Lifetime Measurements. *APL Photonics* **2016**, *1* (4), 046103. https://doi.org/10.1063/1.4948645.

(56) Chen, B.; Yang, M.; Priya, S.; Zhu, K. Origin of J – V Hysteresis in Perovskite Solar Cells. *J. Phys. Chem. Lett.* **2016**, *7* (5), 905–917. https://doi.org/10.1021/acs.jpclett.6b00215.

(57) Menzel, S.; Kaupmann, P.; Waser, R. Understanding Filamentary Growth in Electrochemical Metallization Memory Cells Using Kinetic Monte Carlo Simulations. *Nanoscale* **2015**, *7* (29), 12673–12681. https://doi.org/10.1039/c5nr02258d.

(58) Li, Y.; Zhang, M.; Long, S.; Teng, J.; Liu, Q.; Lv, H.; Miranda, E.; Suñé, J.; Liu, M.

Investigation on the Conductive Filament Growth Dynamics in Resistive Switching Memory via a Universal Monte Carlo Simulator. *Sci. Rep.* **2017**, *7* (1), 11204. https://doi.org/10.1038/s41598-017-11165-5.

(59) Han, J. S.; Le, Q. Van; Choi, J.; Hong, K.; Moon, C. W.; Kim, T. L.; Kim, H.; Kim, S. Y.; Jang, H. W. Air-Stable Cesium Lead Iodide Perovskite for Ultra-Low Operating Voltage Resistive Switching. *Adv. Funct. Mater.* **2018**, *28* (5), 1705783. https://doi.org/10.1002/adfm.201705783.

(60) Sun, Y.; Tai, M.; Song, C.; Wang, Z.; Yin, J.; Li, F.; Wu, H.; Zeng, F.; Lin, H.; Pan, F. Competition between Metallic and Vacancy Defect Conductive Filaments in a $CH_3NH_3PbI_3$-Based Memory Device. *J. Phys. Chem. C* **2018**, *122* (11), 6431–6436. https://doi.org/10.1021/acs.jpcc.7b12817.

(61) Domanski, K.; Correa-Baena, J. P.; Mine, N.; Nazeeruddin, M. K.; Abate, A.; Saliba, M.; Tress, W.; Hagfeldt, A.; Grätzel, M. Not All That Glitters Is Gold: Metal-Migration-Induced Degradation in Perovskite Solar Cells. *ACS Nano* **2016**, *10* (6), 6306–6314. https://doi.org/10.1021/acsnano.6b02613.

(62) Juarez-perez, E. J. Photodecomposition and Thermal Decomposition in Methylammonium Halide Lead Perovskites and Inferred Design Principles to Increase Photovoltaic Device Stability. *J. Mater. Chem. A* **2018**, 9604–9612. https://doi.org/10.1039/c8ta03501f.

(63) Kim, H.; Han, J. S.; Kim, S. G.; Kim, S. Y.; Jang, H. W. Halide Perovskites for Resistive Random-Access Memories. *J. Mater. Chem. C* **2019**, *7* (18), 5226–5234. https://doi.org/10.1039/C8TC06031B.

(64) Du, H.; Jia, C.-L.; Koehl, A.; Barthel, J.; Dittmann, R.; Waser, R.; Mayer, J. Nanosized Conducting Filaments Formed by Atomic-Scale Defects in Redox-Based Resistive Switching Memories. *Chem. Mater.* **2017**, *29* (7), 3164–3173. https://doi.org/10.1021/acs.chemmater.7b00220.

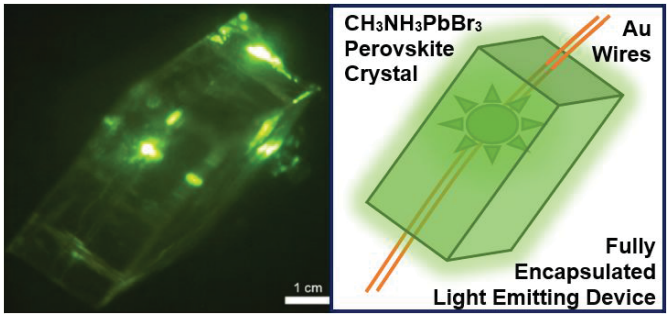
1 cm
$CH_3NH_3PbBr_3$
Perovskite
Crystal
Au
Wires
Fully
Encapsulated
Light Emitting Device